Journal of Clinical Monitoring and Computing manuscript No.
(will be inserted by the editor)

Accurate end systole detection in dicrotic notch-less arterial pressure waveforms.

Joel Balmer · Rachel Smith · Christopher G. Pretty · Thomas Desaive · Geoff M. Shaw · J. Geoffrey Chase

Received: date / Accepted: date

Abstract Identification of end systole is often necessary when studying events specific to systole or diastole, for example, models that estimate cardiac function and systolic time intervals like left ventricular ejection duration. In proximal arterial pressure waveforms, such as from the aorta, the dicrotic notch marks this transition from systole to diastole. However, distal arterial pressure measures are more common in a clinical setting, typically containing no dicrotic notch. This study defines a new end systole detection algorithm, for dicrotic notch-less arterial waveforms. The new algorithm utilises the beta distribution probability density function as a weighting function, which is adaptive based on previous heartbeats end systole locations. Its accuracy is compared with an existing end systole estimation method, on dicrotic notch-less distal pressure waveforms. Because there are no dicrotic notches defining end systole, validating which method performed better is more difficult. Thus, a validation method is developed using dicrotic notch locations from simultaneously measured aortic pressure, forward projected by pulse transit time (PTT) to the more distal pressure signal. Systolic durations, estimated by each of the end systole estimates, are then compared to the validation systolic duration provided by the PTT based end systole point. Data comes from ten pigs, across two protocols testing the algorithms under different hemodynamic states. The resulting mean difference ± limits of agreement between measured and estimated systolic duration, of -8.7 ± 26.6 ms verses -23.2 ± 37.7 ms, for

Joel Balmer
Department of Mechanical Engineering,
University of Canterbury, New Zealand
E-mail: joel.balmer@pg.canterbury.ac.nz

Rachel Smith
Department of Mechanical Engineering,
University of Canterbury, New Zealand

the new and existing algorithms respectively, indicate the new algorithms superiority.

Keywords End systole · Start diastole · Dicrotic notch · Cardiovascular system · Pressure contour interpretation.

1 Introduction

The dicrotic notch is a combination of two turning points with respective local minimum and maximum in arterial pressure signals, found between a beats peak pressure and diastolic relaxation. It is formed by the reflection of a wave off of the aortic valve, following valve closure [1]. Thus, it is clearest in proximal pressure signals and determines transition from systole to diastole [2]. Specifically, aortic systolic duration, associated with left ventricular ejection, lasts from the *foot* of the aortic pressure wave to the dicrotic notch [3–5]. Diastolic duration, associated with ventricular relaxation, is the remaining time from the dicrotic notch to the next pressure waveform foot.

Given the physical significance of the dicrotic notch as a systolic/diastolic time reference, it has been used in numerous applications, including, pulse wave velocity calculations [6], models estimating cardiovascular function [7–12], and left ventricular ejection time. Therefore there are many different algorithms which apply different signal processing methods to dicrotic notch detection [2, 13–16].

Despite the convenience of the dicrotic notch indicating end systole, in a clinical setting, measuring central arterial pressure high in the aorta is not as common as more distal measures, such as in the femoral or iliac arteries. However, as a pressure waveform travels away from the heart, its shape is influenced by changes in vascular properties and reflected waves [2], attenuating the dicrotic notch to a notchless point of inflection or simply a slight change in curvature. This attenuation makes end systole (t_{es}) more difficult to identify in distal pressure waveforms [2]. Additionally, the dicrotic notch shape is known to deteriorate with age [17].

To simplify t_{es} estimation, previous studies have assumed it at the point of maximum negative pressure gradient with respect to time ($\min \frac{dP}{dt}$) [18,8, 19,11], typically occurring between the peak pressure of a beat and before the start of diastolic relaxation. This simplification underestimates systolic duration (T_{sys}) and overestimates diastole [16] but provides consistent predictable performance in signals with and without dicrotic notches.

This study presents a more appropriate method, estimating $t_{es,d^2P/dt^2}$ as a peak in the weighted second derivative ($\frac{d^2P}{dt^2}$). Specifically, the second derivative is weighted so the resulting $\frac{d^2P}{dt^2}$ peak corresponds to the local maximum curvature in the region of downward concavity, making it appropriate for signals with and without dicrotic notches. The accuracy and robustness of the new method is tested on the more difficult dicrotic notch-less signals, increasing its clinical applicability. It is compared to a weighted first derivative method,

$t_{es,dP/dt}$, which is summarized in Appendix A and first published elsewhere [11].

2 Methods

2.1 Ethics statement

Data in this study was obtained from a prior series of pig experiments conducted at the Centre Hospitalier Universitaire de Liège, Belgium. Ethics approval for the experimental procedures, protocols and use of the data was provided by the Ethics Committee of the University of Liège Medical Faculty, permit numbers 1452 & 14-1726 respectively.

2.2 Porcine trial procedures

Data from 10 pure pietrain pigs weighing 18.5–29 kg were used in the analysis, from 2 separate experiments with different experimental protocols. The original intention of each protocol are not relevant to this study. However, the variety of hemodynamic modifications enables testing end systole estimation across a wider range of hemodynamic states and thus pressure waveforms shapes.

Each pig was sedated, anaesthetised and mechanically ventilated with a baseline positive end-expiratory pressure (PEEP) of 5 cmH_2O and tidal volume of 10 $ml\,kg^{-1}$. Both protocols used high fidelity pressure catheters (Transonic, Ithaca, NY, USA) to measure left ventricular (P_{vent}) and proximal aortic pressure (P_{prox}). Dicrotic notch-less distal measures were from the abdominal aorta and femoral artery (P_{dist}), for Protocols 1 and 2 respectively. Data was sampled at 1000Hz for Protocol 1 and 250Hz for Protocol 2.

Pigs 1 – 4 are associated with *Protocol 1*, where a continuous infusion of *dobutamine* modulated heart contractility and can also act as a vasodilator [20,21]. Pig 3 was infused at a rate of 2.5 $\mu g\,kg^{-1}\,min^{-1}$ while Pigs 1, 2 and 4 were infused at 5 $\mu g\,kg^{-1}\,min^{-1}$. This protocol also measured an electrocardiogram (ECG) signal. A full description of the *dobutamine protocol* is available elsewhere [11,22].

Pigs 5 – 10 are associated with *Protocol 2*, characterised by a 30 min infusion of e. coli lipopolysaccharide (*endotoxin*), inducing a septic shock like response: inflammation, capillary leakage, decreased afterload, hypovolemia, tissue hypoxia and eventual cardiac failure [23,24]. A full description of the *endotoxin protocol* is available elsewhere [25].

In both protocols, lung recruitment manoeuvres (RMs) were used, where PEEP is increased in 5 cmH_2O increments up to a maximum of 15 cmH_2O for Pigs 4 and 9, and 20 cmH_2O for all remaining pigs. Increases in PEEP can reduce systemic venous return to the right heart and increase pulmonary resistance. Thus, left ventricle preload decreases, leading to lower arterial pressure [26].

2.3 Data Selection Summary

The data used in the analysis is taken from three distinct *stages* of the two experimental protocols. Thirty heart beats are used for each stage, meaning a total of 900 heart beats are used in the analysis. The equal number of heart beats analysed from each stage, ensures equal representation in statistical comparisons. The *control* stage was when a pig was at rest following anaesthesia, before any hemodynamic modifications were applied. *High PEEP* comes from the RM, specifically during the PEEP level of 15 cmH_2O. Pigs 1 – 4 have the *dobutamine* stage of Protocol 1, where the 30 beats are during the continuous dobutamine infusion. Protocol 2's final stage is *end endo*, which for Pigs 6, 7 and 9 refers to 30 beats just prior to the cessation of the endotoxin infusion. Pigs 5, 8 and 10 responded more dramatically to the endotoxin infusion causing cardiac/circulatory failure before the full 30 min was complete. Therefore, the *end endo* stage for these pigs is during the late part of their rapid decline in hemodynamic stability.

2.4 Weighted second derivative algorithm implementation

In P_{dist}, end systole occurs in the region of downward concavity leading into diastolic decay. Concavity can be measured using the second derivative with respect to time ($\frac{d^2P}{dt^2}$). End systole ($t_{es,d^2P/dt^2}$) corresponds to a prominent peak in $\frac{d^2P}{dt^2}$, in the region after the peak pressure, as shown in Fig 1.

However, noise amplification when calculating discrete data's second derivative, makes this peak more difficult to identify. Although filtering $\frac{d^2P}{dt^2}$ removes most of the noise, noise at a similar frequency to the peak associated with $t_{es,d^2P/dt^2}$ cannot be removed, as seen in Fig 1. Therefore, a weighting function, $w(t)$, is applied to attenuate $\frac{d^2P}{dt^2}$ peaks based on their distance from the region in which t_{es} is expected to occur. The weighting is based on a beta distribution probability density function, which is normalized so its magnitude ranges from 0 to 1. The algorithm implementation is as follows:

1. $\frac{d^2P}{dt^2}$ is calculated and passed through a zero phase delay Hamming low pass filter, with a cut off frequency of 20 Hz and transition width of 5 Hz.
2. Time of start of systole for each beat (t_{foot}) is identified as the feet in the pressure waveform, along with each beats peak pressure ($t_{P_{max}}$). The algorithm used is outlined in Appendix B, and discussed in more detail elsewhere [16,22].
3. The weighting is calculated and applied to each beat individually according to the following:
   (a) The n^{th} beat ($t_{foot,n}$ to $t_{foot,n+1}$) is considered in isolation, so time is with respect to the start of the beat, ranging from 0 to T, where T is the duration of the beat
   (b) The weighting function $w(t)$ is calculated as follows:

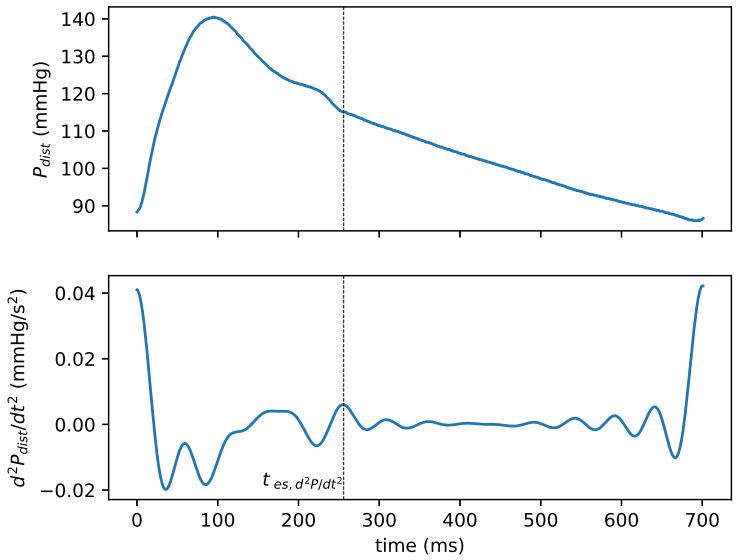

Fig. 1 The rationale for identifying end systole as a prominent peak in the filtered second derivative ($t_{es,d^2P/dt^2}$), corresponding to the transition to start of diastole. This beat is taken from Pig 2's high PEEP stage.

$$w(t) = \begin{cases} 0 & : t \leq t_{P_{max}} \\ \tau^{\alpha-1}(1-\tau)^{\beta-1} & : t > t_{P_{max}} \end{cases} \quad \text{where} \quad \tau(t) = \frac{t - t_{P_{max}}}{T - t_{P_{max}}} \tag{1}$$

Where for $t > t_{P_{max}}$, $w(t)$ becomes a beta distribution probability density function, distributed over the remainder of the beat. With $0 \leq \tau \leq 1$ and $\beta = 5$, the basic shape of $w(t)$ is defined. α allows control over the final shape by shifting its peak, as shown in Fig 2.

α ensures an adaptive beat specific weighting, that places the $w(t)$ peak ($t_{w_{max}}$) in the expected vicinity of t_{es}. α is found according to the following equation:

$$\alpha = \frac{\beta\tau_{w_{max}} - 2\tau_{w_{max}} + 1}{1 - \tau_{w_{max}}} \quad \text{where} \quad \tau_{w_{max}} = \frac{t_{w_{max}} - t_{P_{max}}}{T - t_{P_{max}}} \tag{2}$$

Equation 2 is derived from recognition $\tau_{w_{max}}$ comes from $\frac{dw(t>t_{P_{max}})}{dt} = 0$. Thus, all that is necessary is to define $t_{w_{max}}$ in the location of the expected end systole point (t_{es}) for the n^{th} beat according to the following:

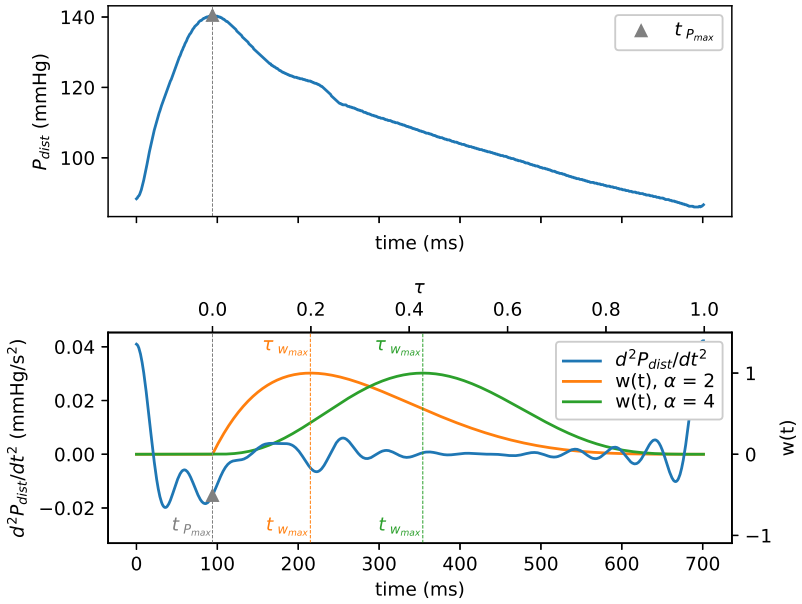

Fig. 2 Same beat as for Fig 1. Two different possible weighting functions are shown, illustrating the effect of α on the weightings peak location, $t_{w_{max}}$ and $\tau_{w_{max}}$ respectively.

i. If $n \leq 3$, an empirical relationship gives an estimate of systolic duration based on heart rate ($T_{sys,HR}$), where HR is in beats per second [27]:

$$t_{w_{max}} = T_{sys,HR} = -0.1\text{HR} + 0.45 \tag{3}$$

where $T_{sys,HR}$ is used to define $t_{w_{max}}$ with respect to the start of the beat.

ii. If n > 3, $t_{w_{max}}$ is the mean systolic duration ($\overline{T_{sys}}$) from the previous three beats identified $t_{es,d^2P/dt^2}$:

$$t_{w_{max}} = \overline{T_{sys}} = \frac{1}{3}\sum_{i=1}^{3} T_{sys,n-i} \tag{4}$$

α is also bound from 1.5 to 4.5, ensuring $t_{w_{max}}$ is not placed too early in systole, or too late in diastole.

4. With $w(t)$ calculated using equation 1, $t_{es,d^2P/dt^2}$ is found as the time of the most prominent peak in the product $w(t)\frac{d^2P}{dt^2}$, the weighted second derivative. The culmination of all steps is shown in Fig 3, using the third and fourth beats of Pig 2's high PEEP stage. This way both steps 3(b)i and 3(b)ii, for $t_{w_{max}}$ determination, are illustrated.

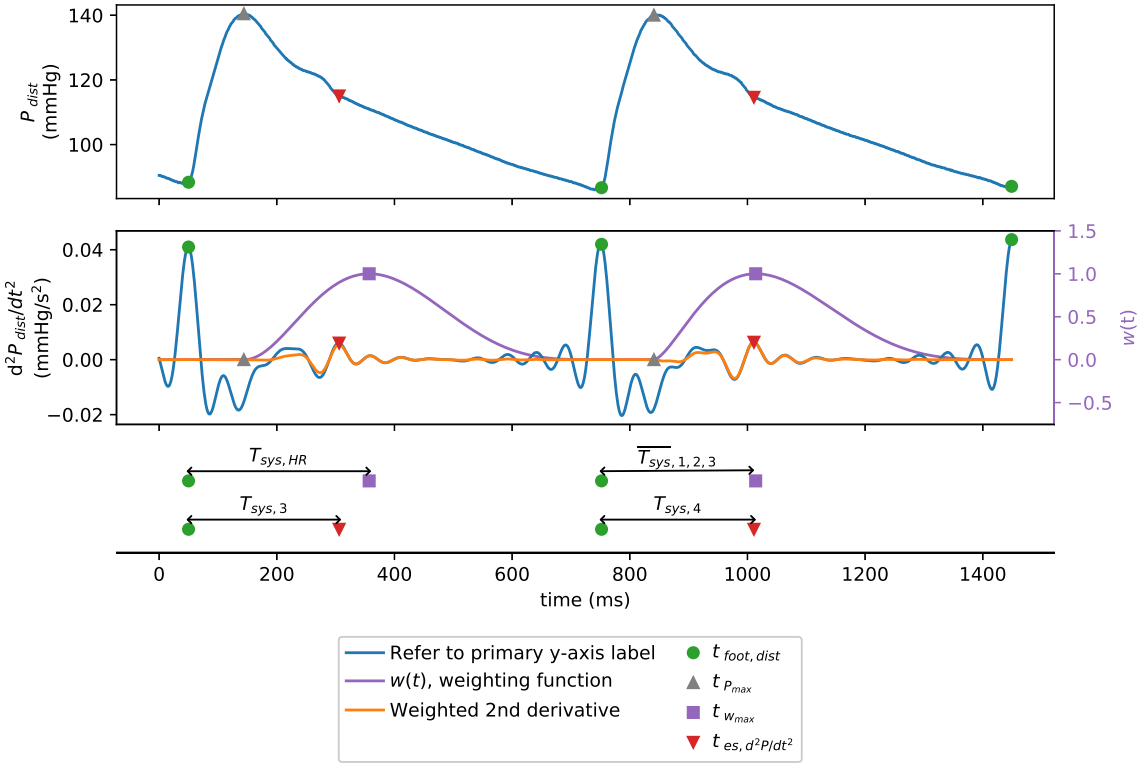

Fig. 3 Example end systole detection, using the 3rd and 4th beats of Pig 2's *high PEEP* stage. Note, beats 1-3 use Equation 3 to define $t_{w_{max}}$ location. Subsequent beats move $t_{w_{max}}$ using the mean systolic duration of the previous three beats, per Equation 4, thus, beat four uses the mean of beats 1-3, $\overline{T_{sys}}_{,1,2,3}$.

5. *As stated in Section 1, $t_{es,d^2P/dt^2}$ identification is easier when dicrotic notches are present, since the associated second derivative peak has much more prominence. However, filtering the second derivative in step 1 will shift the $t_{es,d^2P/dt^2}$ peak due to the removal of some frequency content. To account for this, Appendix C covers an optional additional step specifically for dicrotic notch detection.*

2.5 Validation: forward projection of dicrotic notch location

Since by eye, there is no definitive t_{es} location in a dicrotic notch-less arterial waveform, validation of $t_{es,d^2P/dt^2}$ is more difficult. However, pulse transit

time (PTT), the time taken for the pulse to travel between two arterial sites, provides a physiologically based t_{es} location. PTT is usually measured between the feet of two different pressure measures, such as P_{prox} and P_{dist}, [22]. However, absolute end systole/start diastole, can also be described as wave propagation, with valve closure causing a *forward travelling expansion wave*, reducing pressure as it travels along the arterial tree [28,29]. Fig 4 shows how forward projecting a known end systole point, by PTT, accurately predicts the time end systole is experienced at the downstream arterial site. Thus, $t_{es,PTT}$, is found by forward projecting the dicrotic notch location, from P_{prox}, by PTT, onto the the P_{dist} signal, as shown in Fig 5. However, $t_{es,PTT}$ is *not* definitive, since the approach negates the effects of the changing waveform shape as it travels along the arterial tree [30]. The changing waveform shape is partly due to reflected wave phenomena, but also due to the relationship between wave propagation velocity and pressure [31]. Specifically, because the pressure at end-systole is higher than start-systole, it is possible the wave propagation of end-systole is faster than start-systole. Thus, $t_{es,PTT}$ could slightly overestimate the true end-systole location in distal pressure waveforms. Additionally, since $t_{es,PTT}$ requires two arterial pressure signals, it is unlikely to be viable in a clinical setting. However, it still provides a means of validating which of $t_{es,dP/dt}$ and $t_{es,d^2P/dt^2}$ is the better estimate.

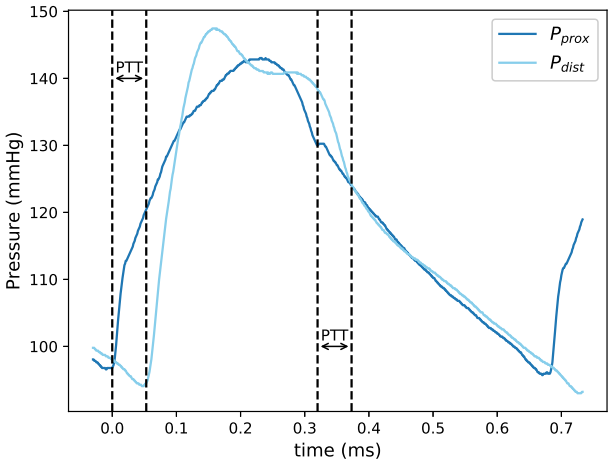

Fig. 4 Example of how pulse transit time (PTT) describes the propagation of the pressure disturbance associated with end systole/start diastole along the arterial tree, marking the transition from late systole into diastolic pressure decay.

Dicrotic notch detection ($t_{es,dic}$) in P_{prox} was performed using an established adaptive shear transform method, similar to that used for foot detection

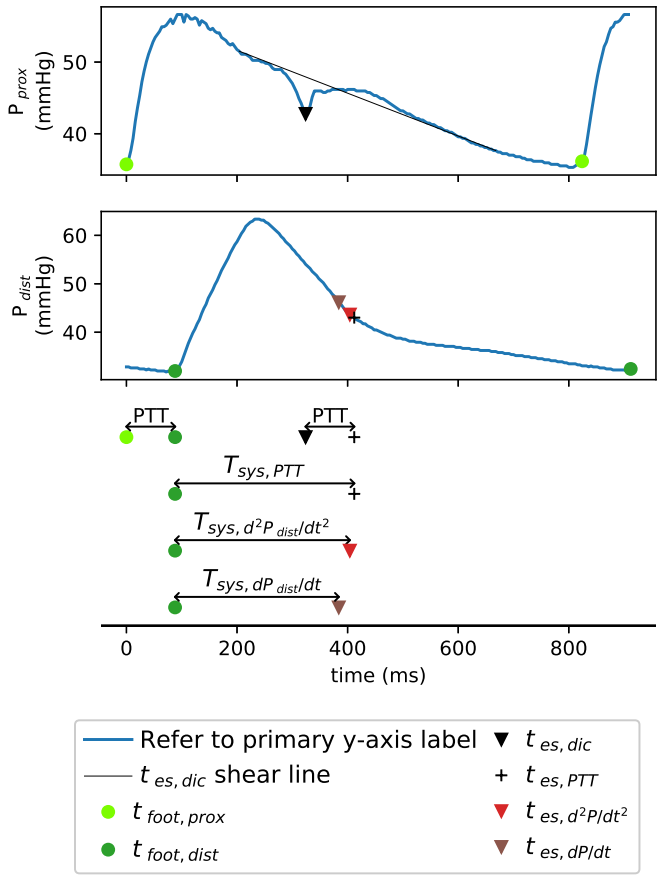

Fig. 5 Example of how pulse transit time (PTT) was used to compare the t_{es} algorithms using T_{sys} estimates. The example uses pressure waveforms from Pig 9's control stage.

in Fig 9. An example of the shear line used is shown in Fig 5 but its detailed construction is discussed elsewhere [16]. In addition, using 30 beats for each pig and stage, made checking the dicrotic notch detection in P_{prox} simple to facilitate by eye.

2.6 Analyses

Rather than directly comparing the difference between the derivative based end systole estimates ($t_{es,dP/dt}$ & $t_{es,d^2P/dt^2}$) and $t_{es,PTT}$, their resulting sys-

tolic durations are compared. The three systolic durations are shown in Fig 5 and summarized below with their respective end systole estimates:

- $T_{sys,PTT}$, where end of systole is $t_{es,PTT}$
- $T_{sys,dP/dt}$, where end systole is $t_{es,dP/dt}$
- $T_{sys,d^2P/dt^2}$, where end systole is $t_{es,d^2P/dt^2}$

T_{sys} is used because, as discussed in the Section 1, end systole is often found to determine systolic and diastolic time intervals [3–5].

The accuracy of $T_{sys,dP/dt}$ and $T_{sys,d^2P/dt^2}$ compared with $T_{sys,PTT}$, are analysed using two formats. Correlation plots show the overall regression line and coefficient of determination (r^2) for the pigs. The coefficient of determination, r^2, represents the fraction of the total observed variation in $T_{sys,d^2P/dt^2}$ or $T_{sys,dP/dt}$, due to the observed variation in $T_{sys,PTT}$. However, correlation does not imply agreement [32] and therefore Bland-Altman analysis is also used.

3 Results & Discussion

3.1 Correlation outcomes

Overall correlations shown in Fig 6a & 6b, $r^2 = 0.77$ versus 0.87 respectively, suggest more of the variability in $T_{sys,d^2P/dt^2}$ is explained by $T_{sys,PTT}$, compared with $T_{sys,dP/dt}$. However, Pig 5 and Pig 8 have individual coefficients of determination for $T_{sys,dP/dt}$ higher than for $T_{sys,d^2P/dt^2}$, shown in Table 1. These two higher r^2 values can be misleading if used to assess agreement [32], since for Pig 5, $t_{es,d^2P/dt^2}$ was closest to $t_{es,PTT}$ for 87 of its 90 beats, with only 3 beats during *end endo* where $t_{es,dP/dt}$ was closer to $t_{es,PTT}$. Similarly $t_{es,d^2P/dt^2}$ was the better estimate in 17 of 30 beats in Pig 8 *end endo*.

As stated in Section 2.3, inadequate pulse pressures led to circulatory failure prior to the full 30 minutes of endotoxin infusion in Pigs 5 and 8. This is to blame for the reduction in end systole detection accuracy and outliers in Figures 6 and 7. Specifically, Pig 8's femoral pressure fell to a mean value of 24 mmHg, with a pulse pressure of only a few millimetres of mercury, at which point the effectively non-pulsatile signal makes end systole detection difficult for either algorithm. Since P_{prox} was maintained longer than P_{dist} during the *end endo* stage, a dicrotic notch still enabled reasonable $t_{es,PTT}$ estimation.

3.2 Bland Altman outcomes

Fig 7 shows the mean systematic error of the weighted second derivative method was lower than its weighted first derivative counterpart, -8.7 ms verse -23.2 ms respectively. Additionally, the new algorithm has narrower limits of agreement (mean ± 1.96 standard deviations), of ±26.6 ms verses ±37.7 ms, confirming across all pigs and stages its superiority over the old algorithm.

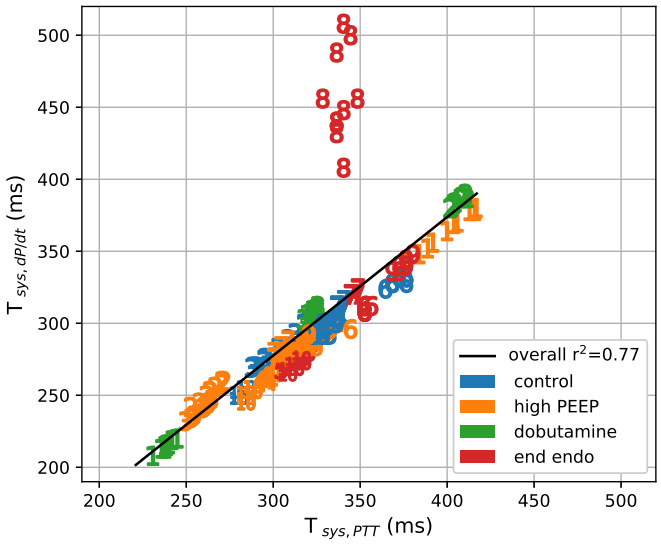

(a) Variation in $T_{sys,dP/dt}$ described by $T_{sys,PTT}$

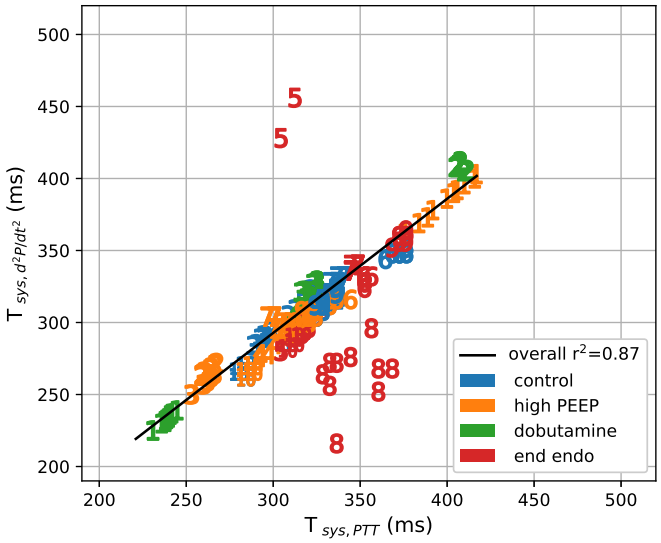

(b) Variation in $T_{sys,d^2P/dt^2}$ described by $T_{sys,PTT}$

Fig. 6 The overall coefficient of determination (round to 2 d.p.), for both $T_{sys,dP/dt}$ (a) and $T_{sys,d^2P/dt^2}$ (b) estimation methods. The data points are numbered, corresponding to the pig they represent. The ten beats of highest error are shown for each pigs stage, to improve clarity.

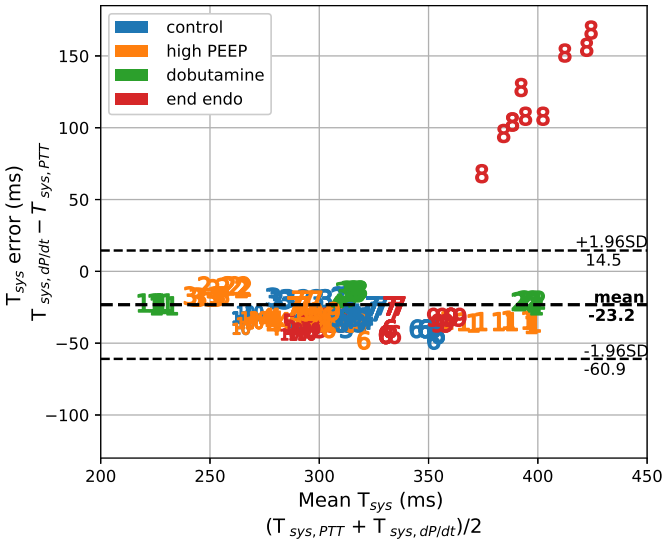

(a) Agreement between $T_{sys,dP/dt}$ and $T_{sys,PTT}$

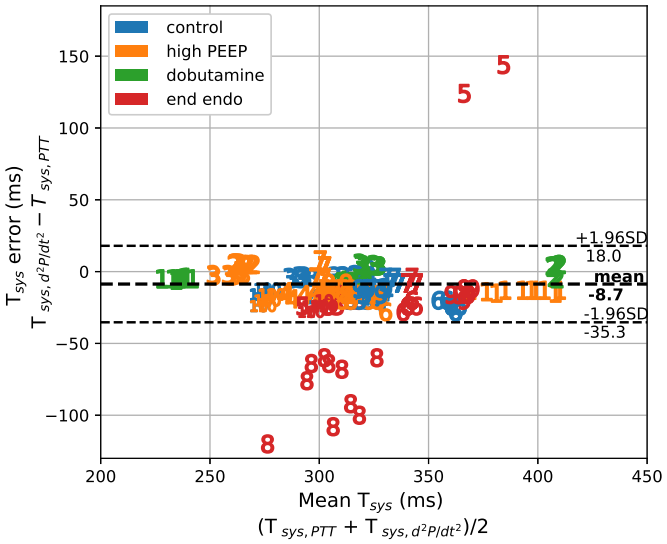

(b) Agreement between $T_{sys,d^2P/dt^2}$ and $T_{sys,PTT}$

Fig. 7 Bland-Altman analysis, where the mean bias between $T_{sys,PTT}$ and the derivative based T_{sys} estimates are shown, as well as the limits of agreement. The data points are numbered, corresponding to the pig they represent. The ten beats of highest error are shown for each pigs stage, to improve clarity.

Table 1 Coefficient of determination (r^2) for each T_{sys} estimate ($T_{sys,dP/dt}$ & $T_{sys,d^2P/dt^2}$) vs $T_{sys,PTT}$, for each individual pig (rounded to 2 d.p.).

	Pig									
	1	**2**	**3**	**4**	**5**	**6**	**7**	**8**	**9**	**10**
$\boldsymbol{T_{sys,dP/dt}}$	1.0	1.0	0.99	0.83	0.59	0.93	0.98	0.44	0.98	0.87
$\boldsymbol{T_{sys,d^2P/dt^2}}$	1.0	1.0	0.99	0.83	0.01	0.94	0.97	0.0	0.98	0.87

Notably, ignoring Pig 8's *end endo* stage outliers, explained in Section 3.1, $t_{es,dP/dt}$ consistently underestimates systolic duration, with all data points in Fig 7a being less than zero, ensuring negative mean bias. This limitation is expected, due to the first derivative trough (seen in Fig 8) describing a point of maximum negative gradient, as opposed to a stationary point. Figures 5 and 8 show this max negative gradient lies between $t_{P_{max}}$ and $t_{es,PTT}$, with the magnitude of the gradient reducing through $t_{es,PTT}$ and into diastole. Similar results have been published for the same analysis assessing the weighted first derivative algorithms dicrotic notch detection in aortic pressure signals [16].

In contrast, the weighting in the second derivative algorithm is developed specifically to estimate the location of an attenuated dicrotic notch. Interestingly, despite this improvement, $T_{sys,d^2P/dt^2}$ still averaged 8.7 ms shorter than $T_{sys,PTT}$, as shown in Figure 7b. However, this *may not* necessarily reflect error in $t_{es,d^2P/dt^2}$, but is possibly the error in $t_{es,PTT}$ hypothesised in Section 2.5. Specifically, $t_{es,PTT}$ may slightly overestimate the true location of t_{es} in the distal pressure waveform, due to a higher wave speed being expected at the higher end-systole pressures relative to start-systole. Regardless, the results indicate, despite no dicrotic notch being present, physiologically based end systole detection is still possible, without compromising accuracy by using the first derivative method. More importantly, the $t_{es,d^2P/dt^2}$ approach improves clinical applicability of other algorithms and methods that require end systole detection as an input [33].

3.3 End systole detection limitations

The study is generalizable to human arterial signals measured from the proximal aorta to the femoral artery. However, a reduction in performance may occur in even more peripheral arterial signals, where reflected waves can cause turning points that appear similar to a dicrotic notch but do not correspond to end systole, for example in the radial artery [2,14]. The algorithm has not yet been tested on such peripheral signals as this study extends only as far as the femoral artery, which is readily accessible in intensive care and similar clinical situations [34,35], and is less prone to wave reflection induced distortions [30].

This study used a range of hemodynamic states found in an intensive care setting, including recruitment manoeuvres, dobutamine admission and septic shock like response. While this diversity ensured both stable and unstable

hemodynamics were tested, it is possible other behaviour not tested could cause issues. For example, cardiac arrhythmia can significantly alter expected pressure waveform shape beat-to-beat. It is likely the algorithm presented in this study would suffer reduced performance under these conditions. However, in a clinical setting, severe cardiac arrhythmia would not be left unresolved and end systole detection under such conditions is unlikely of immediate clinical need or interest.

4 Conclusions

The study develops a simple end systole detection algorithm for use in dicrotic notch-less arterial pressure waveforms, that improved end systole detection over an existing method. The results showed the new adaptively weighted second derivative method was better able to track changes in systolic duration, with less bias and narrower limits of agreement, when compared with the existing method (-8.7 ± 26.6 ms verses -23.2 ± 37.7 ms).

Acknowledgements This study was supported with funding from Medtech CoRE, Royal Society of New Zealand Cook Fellowship and the Ministry of Business and Innovation (via National Science Chellenge). The funders had no role in study design, data collection and analysis, decision to publish or preparation of the manuscript.

Conflicts of interest

The authors declare that they have no conflicts of interest.

References

1. T. Lewis, "The factors influencing the prominence of the dicrotic wave," *J. Physiol.*, vol. 34, no. 6, pp. 414–429, 1906.
2. M. J. Oppenheim and D. F. Sittig, "An Innovative Dicrotic Notch Detection Algorithm Which Combines Rule-Based Logic with Digital Signal Processing Techniques," *Comput. Biomed. Res.*, vol. 28, no. 2, pp. 154–170, 1995.
3. R. C. Talley, J. F. Meyer, and J. L. McNay, "Evaluation of the pre-ejection period as an estimate of myocardial contractility in dogs," *Am. J. Cardiol.*, vol. 27, pp. 384–391, apr 1971.
4. R. A. Payne, C. N. Symeonides, D. J. Webb, and S. R. J. Maxwell, "Pulse transit time measured from the ECG: an unreliable marker of beat-to-beat blood pressure," *J. Appl. Physiol.*, vol. 100, pp. 136–141, jan 2006.
5. P. E. Marik, "Noninvasive cardiac output monitors: A state-of the-art review," *J. Cardiothorac. Vasc. Anesth.*, vol. 27, no. 1, pp. 121–134, 2013.
6. E. Hermeling, K. D. Reesink, L. M. Kornmann, R. S. Reneman, and A. P. Hoeks, "The dicrotic notch as alternative time-reference point to measure local pulse wave velocity in the carotid artery by means of ultrasonography," *J. Hypertens.*, vol. 27, pp. 2028–2035, oct 2009.
7. J.-J. Wang, A. B. O'Brien, N. G. Shrive, K. H. Parker, and J. V. Tyberg, "Time-domain representation of ventricular-arterial coupling as a windkessel and wave system," *Am. J. Physiol. - Hear. Circ. Physiol.*, vol. 284, no. 4, pp. H1358–H1368, 2003.

8. J. Aguado-Sierra, J. Alastruey, J.-J. Wang, N. Hadjiloizou, J. Davies, and K. H. Parker, "Separation of the reservoir and wave pressure and velocity from measurements at an arbitrary location in arteries," *Proc. Inst. Mech. Eng. Part H J. Eng. Med.*, vol. 222, pp. 403–416, apr 2008.
9. D. Stevenson, C. Hann, G. Chase, J. Revie, G. Shaw, T. Desaive, B. Lambermont, A. Ghuysen, P. Kolh, and S. Heldmann, "Estimating the driver function of a cardiovascular system model," in *UKACC Int. Conf. Control 2010*, vol. 2010, pp. 1008–1013, Institution of Engineering and Technology, 2010.
10. D. Stevenson, J. Revie, J. G. Chase, C. E. Hann, G. M. Shaw, B. Lambermont, A. Ghuysen, P. Kolh, and T. Desaive, "Beat-to-beat estimation of the continuous left and right cardiac elastance from metrics commonly available in clinical settings," *Biomed. Eng. Online*, vol. 11, no. 1, p. 73, 2012.
11. S. Kamoi, C. Pretty, J. Balmer, S. Davidson, A. Pironet, T. Desaive, G. M. Shaw, and J. G. Chase, "Improved pressure contour analysis for estimating cardiac stroke volume using pulse wave velocity measurement," *Biomed. Eng. Online*, vol. 16, no. 1, p. 51, 2017.
12. J. Balmer, C. Pretty, S. Davidson, T. Desaive, S. Habran, and J. G. Chase, "Effect of arterial pressure measurement location on pulse contour stroke volume estimation , during a rapid change in hemodynamic state," *10th IFAC Symp. Biol. Med. Syst.*, vol. 51, no. 27, pp. 162–167, 2018.
13. K. Takazawa, N. Tanaka, K. Takeda, F. Kurosu, and C. Ibukiyama, "Underestimation of vasodilator effects of nitroglycerin by upper limb blood pressure," in *Hypertension*, 1995.
14. S. Hoeksel, J. R. C. Jansen, J. A. Blom, and J. J. Schreuder, "Detection of Dicrotic Notch in Arterial Pressure Signals," *J. Clin. Monit.*, vol. 13, no. 5, pp. 309–316, 1997.
15. D. Stevenson, J. Revie, J. Chase, C. E. Hann, G. M. Shaw, B. Lambermont, A. Ghuysen, P. Kolh, and T. Desaive, "Algorithmic processing of pressure waveforms to facilitate estimation of cardiac elastance," *Biomed. Eng. Online*, vol. 11, no. 1, p. 28, 2012.
16. J. Balmer, C. Pretty, A. Amies, T. Desaive, and J. G. Chase, "Accurate dicrotic notch detection using adaptive shear transforms," *10th IFAC Symp. Biol. Med. Syst.*, vol. 51, no. 27, pp. 74–79, 2018.
17. T. R. Dawber, H. E. Thomas, and P. M. McNamara, "Characteristics of the Dicrotic Notch of the Arterial Pulse Wave in Coronary Heart Disease," *Angiology*, vol. 24, pp. 244–255, apr 1973.
18. F. L. Abel, "Maximal negative dP/dt as an indicator of end of systole," *Am. J. Physiol. - Hear. Circ. Physiol.*, vol. 240, no. 4, pp. H676—-H679, 1981.
19. S. Kamoi, C. Pretty, P. Docherty, D. Squire, J. Revie, Y. S. Chiew, T. Desaive, G. M. Shaw, and J. G. Chase, "Continuous Stroke Volume Estimation from Aortic Pressure Using Zero Dimensional Cardiovascular Model: Proof of Concept Study from Porcine Experiments," *PLoS One*, vol. 9, p. e102476, jul 2014.
20. R. R. Ruffolo, "Review: The Pharmacology of Dobutamine," *Am. J. Med. Sci.*, vol. 294, pp. 244–248, oct 1987.
21. T. J. Ellender and J. C. Skinner, "The Use of Vasopressors and Inotropes in the Emergency Medical Treatment of Shock," *Emerg. Med. Clin. North Am.*, vol. 26, pp. 759–786, aug 2008.
22. J. Balmer, C. Pretty, S. Davidson, T. Desaive, S. Kamoi, A. Pironet, P. Morimont, N. Janssen, B. Lambermont, G. M. Shaw, and J. G. Chase, "Pre-ejection period, the reason why the electrocardiogram Q-wave is an unreliable indicator of pulse wave initialization," *Physiol. Meas.*, vol. 39, p. 095005, sep 2018.
23. H. B. Nguyen, E. P. Rivers, F. M. Abrahamian, G. J. Moran, E. Abraham, S. Trzeciak, D. T. Huang, T. Osborn, D. Stevens, and D. A. Talan, "Severe Sepsis and Septic Shock: Review of the Literature and Emergency Department Management Guidelines," *Ann. Emerg. Med.*, vol. 48, p. 54.e1, jul 2006.
24. M. W. Merx and C. Weber, "Sepsis and the heart," *Br. J. Anaesth.*, vol. 104, no. 1, pp. 3–11, 2010.
25. S. Davidson, C. Pretty, A. Pironet, T. Desaive, N. Janssen, B. Lambermont, P. Morimont, and J. G. Chase, "Minimally invasive estimation of ventricular dead space volume through use of Frank-Starling curves," *PLoS One*, vol. 12, p. e0176302, apr 2017.

26. T. Luecke and P. Pelosi, "Clinical review: Positive end-expiratory pressure and cardiac output," *Crit. Care*, vol. 9, no. 6, pp. 607–621, 2005.
27. V. Gemignani, E. Bianchini, F. Faita, M. Giannoni, E. Pasanisi, E. Picano, and T. Bombardini, "Assessment of cardiologic systole and diastole duration in exercise stress tests with a transcutaneous accelerometer sensor," in *2008 Comput. Cardiol.*, vol. 35, pp. 153–156, IEEE, sep 2008.
28. J. P. Mynard and J. J. Smolich, "Wave potential and the one-dimensional windkessel as a wave-based paradigm of diastolic arterial hemodynamics," *Am. J. Physiol. Circ. Physiol.*, vol. 307, no. 3, pp. H307–H318, 2014.
29. J. P. Mynard and J. J. Smolich, "Wave potential: A unified model of arterial waves, reservoir phenomena and their interaction," *Artery Res.*, vol. 18, pp. 55–63, 2017.
30. N. Westerhof, N. Stergiopulos, and M. I. M. Noble, "Transfer of Pressure - Snapshots of Hemodynamics: An Aid for Clinical Research and Graduate Education," in *Snapshots of Hemodynamics: An Aid for Clinical Research and Graduate Education* (N. Westerhof, N. Stergiopulos, and M. I. M. Noble, eds.), pp. 189–195, Boston, MA: Springer US, 2010.
31. L. A. Geddes, M. H. Voelz, C. F. Babbs, J. D. Bourland, and W. A. Tacker, "Pulse transit time as an indicator of arterial blood pressure," *Psychophysiology*, vol. 18, no. 1, pp. 71–74, 1981.
32. J. M. Bland and D. Altman, "Statistical Methods for Assessing Agreement Between Two Methods of Clinical Measurement," *Lancet*, vol. 327, pp. 307–310, feb 1986.
33. J. Balmer, C. G. Pretty, S. Davidson, T. Mehta-Wilson, T. Desaive, R. Smith, G. M. Shaw, and J. G. Chase, "Clinically applicable model-based method, for physiologically accurate flow waveform and stroke volume estimation," *Comput. Methods Programs Biomed.*, p. 105125, 2019.
34. T. R. Cousins and J. M. O'Donnell, "Arterial cannulation: A critical review," 2004.
35. C. A. Watson and M. B. Wilkinson, "Monitoring central venous pressure, arterial pressure and pulmonary wedge pressure," *Anaesth. Intensive Care Med.*, vol. 13, no. 3, pp. 116–120, 2012.

Appendices

A The weighted first derivative method for $t_{es,dP/dt}$

The method of finding $t_{es,dP/dt}$ is shown in Fig 8. The weighting is calculated and applied to each beat individually, considering the start of each beat to be time zero. The weighting is calculated according to the following:

$$w(t) = \frac{\left(0.5 - \left|0.5 - \frac{t}{T}\right|\right)^2}{0.25} \quad \text{where} \quad 0 \leq t \leq T \tag{5}$$

Where T is the beat duration. This method is taken from [11], with the addition of the 0.25 denominator to normalized the function ($0 \leq w(t) \leq 1$).

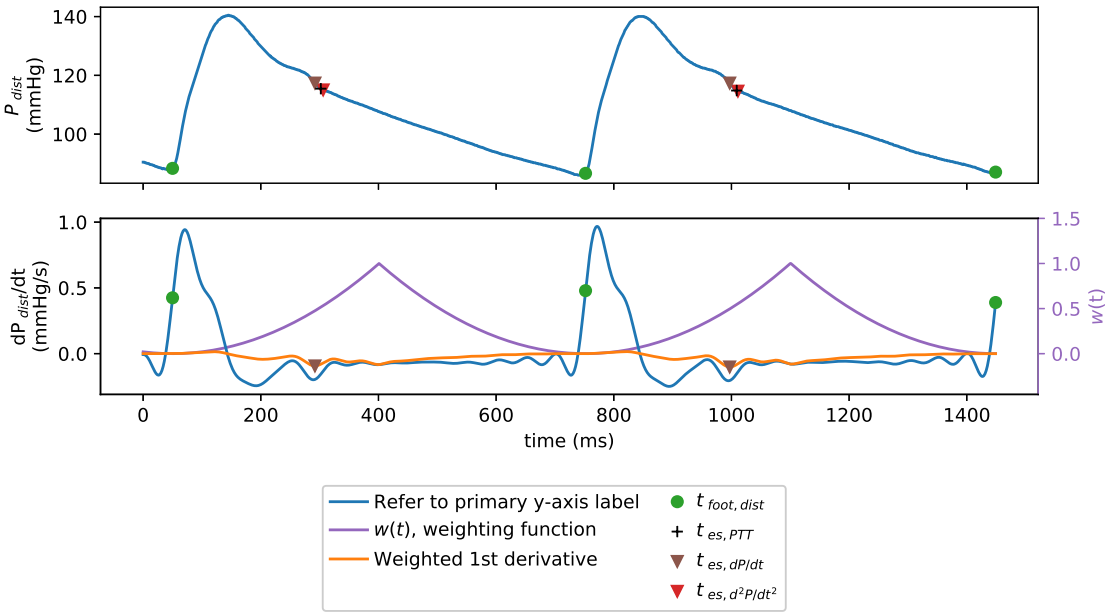

Fig. 8 Example of the weighted first derivative method used to find $t_{es,dP/dt}$, using the same beats as shown in Fig 3. $t_{es,d^2P/dt^2}$ points from Fig 3, and $t_{es,PTT}$ reference points, are also shown for comparison.

B Start systole detection

Start of systole for P_{prox} and P_{dist} was identified as the feet of the waveform according to Fig 9.

First, the approximate start time of ventricular contraction was identified for a beat as either the ECG R-wave (Protocol 1 pigs) or the foot of the P_{vent} waveform (Protocol 2 pigs). Before P_{vent} feet could be found, minima ($P_{vent,min}$) and maxima ($P_{vent,max}$)

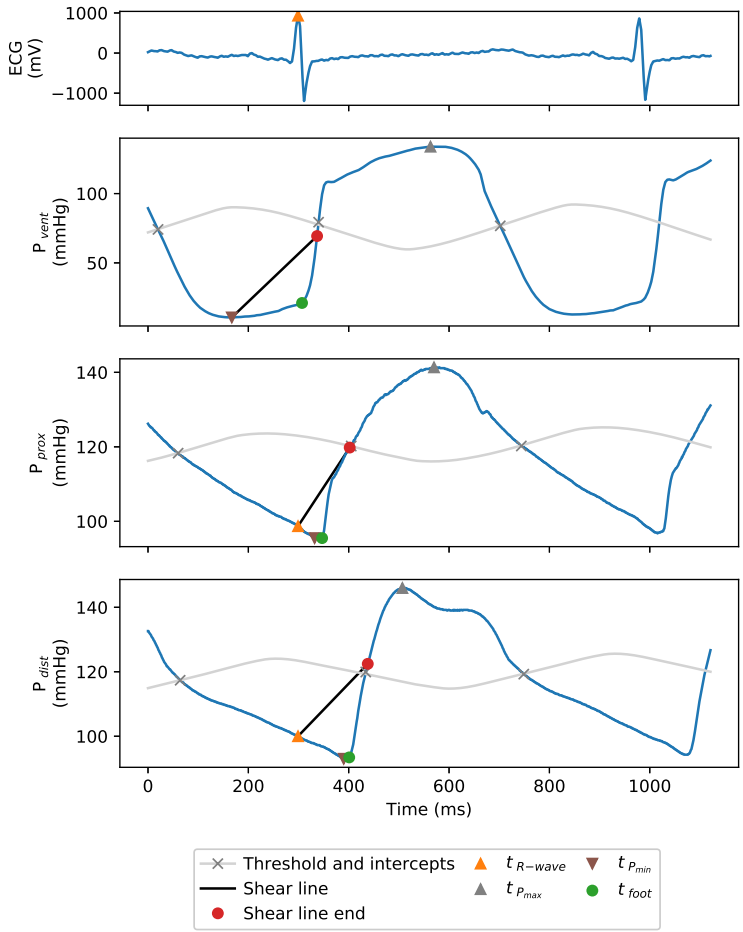

Fig. 9 Example of how start systole is found as the feet of the pressure waveforms. The example uses a beat from Pig 2's control stage. Thus, as a Protocol 1 pig, the ECG R-wave is used to define shear line start when identifying P_{prox} and P_{dist} feet.

were required. These were found between the intercepts of the waveform with a moving mean of window length 1 s, as shown in Fig 9 [16]. A shear line was then constructed from each $P_{vent,min}$ to a point whose pressure was halfway between $P_{vent,min}$ and the next $P_{vent,max}$. A foot is then found under each shear line, as the point with maximum vertical displacement from the shear line. This is equivalent to the minima after shear transforming the segment under the shear line.

Once the start time of ventricular contraction was identified, it served as the shear line start point in identifying P_{prox} and P_{dist} feet. The shear line end point and feet are then identified in the same manner as for P_{vent}. This method of start systole detection is discussed in further detail elsewhere [22].

C Finding $t_{es,d^2P/dt^2}$ in signals with dicrotic notches

As outlined in Section 1, the second derivative peak associated with a dicrotic notch has significant peak prominence, due to abrupt changes in curvature. Thus, when applying the method to proximal or distal signals with dicrotic notches, $t_{es,d^2P/dt^2}$ peak detection is easier, as shown in Fig 10.

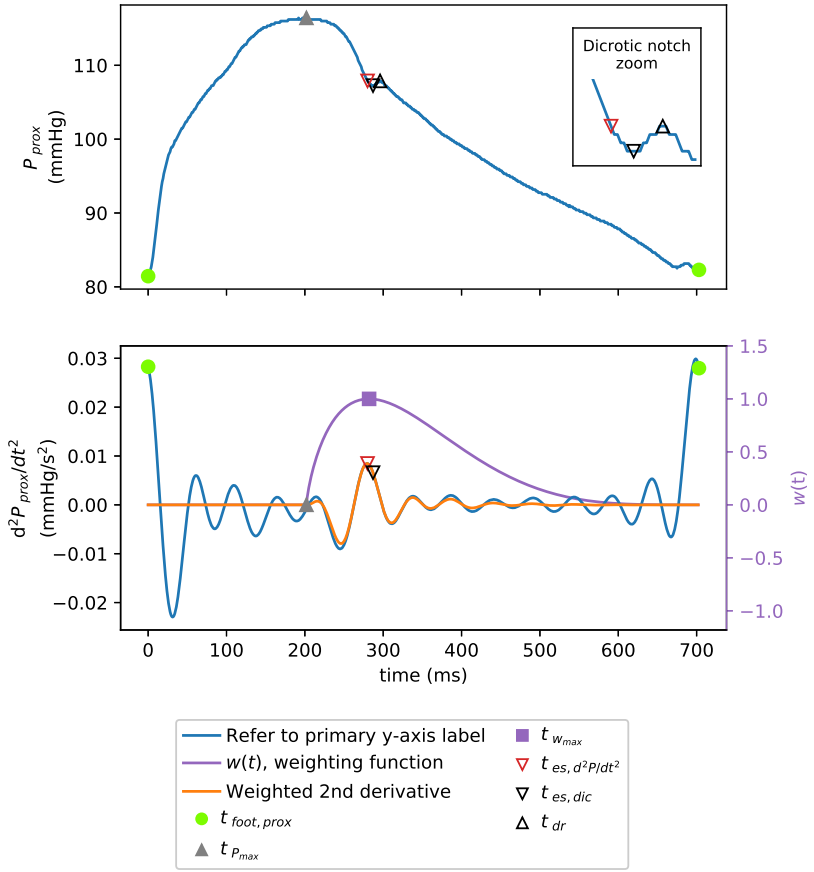

Fig. 10 Example of $t_{es,d^2P/dt^2}$ detection in a pressure waveform with a dicrotic notch. The example uses a proximal pressure waveform from Pig 3's control stage.

However, due to filtering removing some frequency content from the second derivative, $t_{es,d^2P/dt^2}$ may no longer be the very bottom of the dicrotic notch. The degree of error depends on the filter properties and the dicrotic notch shape, and in most applications would be negligible. For example, when applying the second derivative method to P_{prox}, the error between $t_{es,d^2P/dt^2}$ and $t_{es,dic}$ was less than 9 ms for all pigs stages. The exception

being Pig 8's end endo stage, whose maximum shift was 24 ms due to wide dicrotic notches at the low mean proximal aortic pressure of only 20 mmHg.

However, if this error is undesirable, the bottom of the notch can be found with an additional step: A local maxima in pressure following $t_{es,d^2P/dt^2}$ is the second turning point associated with a dicrotic notch and marks the start of *diastolic relaxation* (t_{dr}). To find end systole as the bottom of a dicrotic notch, $t_{es,dic}$, can be defined as the minimum pressure between $t_{P_{max}}$ and t_{dr} as seen more clearly in the zoomed panel of Fig 10. Alternatively, when dicrotic notch presence is known *a priori*, the dicrotic notch detection algorithm presented in [16] and used in this study to identify $t_{es,dic}$, can be used.